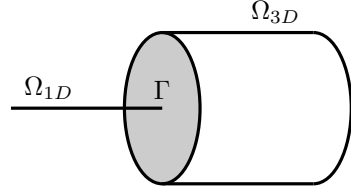


Geometric Multi-Scale Coupling

Partitioned Fluid-Structure Interaction and Multiphysics Simulations

Elia Zonta

Department of Informatics
Technical University of Munich
Email: elia.zonta@tum.de



Abstract—Simulations are more and more heavily employed in science and industry alike. Therefore, the growing demand for computational power requires simulations to be as economic as possible and it is highly desirable to decrease their computational cost without compromising the fidelity of their results. Geometric multi-scale models, i.e., dimensionally heterogeneous, partitioned multi-physics simulations are a potential way of flexibly managing the complexity of simulations. Examples from nuclear engineering and blood flow dynamics are presented to demonstrate the capabilities of geometric multi-scale coupling. Numerical particularities are addressed, especially with regard to 1D-3D computational fluid dynamics simulations. A simplistic 1D-3D flow simulation is conducted and analysed, to exemplify geometric multi-scale coupling and showcase possible pitfalls. Overall, geometric multi-scale models proved very flexible and versatile, but are not unsusceptible to possible oversight that can lead to less accurate models.

Index Terms—Geometric Multi-Scale, Multi-Physics, Partitioned Simulations, Computational Fluid Dynamics, Hemodynamics, Nuclear Engineering

I. INTRODUCTION

Ever since their advent, simulations have been conspicuous in science and engineering. Compared to experimental setups, they were significantly cheaper, easier to execute and enabled the risk- and disruption-free exploration of various systems of interest. In light of the ongoing digitalization and the implementation of *Industry 4.0*, simulation technologies will prove crucial and related research in industrial settings has been steadily increasing over the last four years. [1]

With increasingly complex systems, large-scale simulations oftentimes need to resort to certain simplifications, which impede the achievable accuracy. Geometric multi-scale coupling aims to alleviate this problem by introducing more sophisticated models to the simulation, albeit in an economic manner – they are only employed for effects not accounted for by the reduced model. This allows for partitioned simulations that overall require less computational cost, while still producing feasible results. These partitioned simulations are also highly flexible and modular, since different partitions can theoretically be exchanged, refined or removed from the overall model.

Hence, geometric multi-scale coupling enables the combination of models of varying fidelity – for regions that require higher dimensionality – into a single simulation of the whole system, as illustrated by Figure 1. Naturally, this poses some compelling questions regarding its technical aspects. Those aspects include, e.g., the data mapping approach taken to

Fig. 1: A one-dimensional model of a cylindrical pipe coupled to a three-dimensional one in order to illustrate the general idea of geometric multi-scale coupling. The interface is denoted as Γ and is shown in gray.

project values from the higher-dimensional model onto the lower dimensional one or the interface coupling conditions, that determine the behavior on the border between separate models. Thus, the following paper aims to examine the usage and applications of geometric multi-scale coupling, as well as investigate the theoretical background of geometric multi-scale models based on selected examples.

II. MOTIVATING EXAMPLES

A. Nuclear Reactor Safety

Assessing the safety of nuclear power plants is an indispensable task that heavily relies on simulation data, especially considering the emergence of new plant designs and never before seen technologies. Therefore, the results ought to stem from reliable predictive models in order to enable the responsible persons to implement correct safety margins and obey safety regulations. Currently, system thermal hydraulic codes, such as ATHLET [2] or CATHARE [3], are frequently used to model the entirety of a nuclear power plant with its numerous individual subsystems. These system thermal hydraulic codes, however, tend to be one-dimensional and therefore fail to produce high fidelity results if three-dimensional phenomena significantly affect the behavior of the nuclear power plant. This is the case for larger pools of water that can, for example, be found at certain inlets where flows might circulate. Modeling these areas via single-phase computational fluid dynamics has proven very promising. [4]

Zanetti et al. [5] reproduced Molten Salt Reactor experiments using a geometric multi-scale model implemented in COMSOL Multiphysics® and MATLAB® Simulink. A Molten Salt Reactor is a modern type of nuclear reactor that circulates molten fuel through its core and multiple heat exchangers, with the fuel consisting of fluoride salts containing fissile material

in this case. This technology is often considered to be more sustainable and generally safer, due to the reactor being operated at almost atmospheric pressure, and it might also provide a way of better managing and even reducing radioactive waste. [6] The proposed model entails a multi-physics description of the reactor core, with a number of partial differential equations that are implicitly coupled and solved node-wise in three dimensions to yield accurate values for the heat transport, fluid dynamics and delayed neutron precursor convection. The out-of-core components, i.e., downcomer, heat exchangers and reactor plena, are described by zero-dimensional equations and provide the boundary conditions to the aforementioned core model. By comparison to the experimental results, it could be shown that the predictions are adequate and geometric multi-scale models can be fruitfully used for assessing a large part of the dynamic range of the system. [5]

B. Hemodynamics

Cardiovascular disease is the leading cause of death worldwide and is the most lethal noncommunicable disease, accounting for nearly half of all deaths due to noncommunicable diseases. However, a lot of these deaths occur prematurely and could oftentimes be prevented. [7] Therefore, deepening the understanding of cardiovascular pathophysiology with simulation results is an essential step in developing novel treatment approaches, with the final goal being a reduction of the global disease burden related to cardiovascular disease. Another potential aspect of numerical hemodynamics simulations is the possibility to adjust therapy to the individual patient, by determining patient-specific data, which would eliminate the need to base medical decisions on population means.

The incompressible Navier-Stokes equations in combination with a mathematical description of the deformation of the vascular walls would provide detailed insight into blood flow dynamics. However, the computational cost involved would be too immense for this method to be feasible for larger vascular structures, not to mention the whole vascular system. This is why, analogously to the previous section, lower-dimensional, reduced models are introduced to replace parts of the costly three-dimensional model. Single vessels can be approximated by reducing them to their axial coordinate, effectively yielding a one-dimensional model adhering to the Euler equations. Networks of vessels can be reduced even further by making use of the Kirchhoff laws for hydraulic networks, which results in a zero-dimensional or *lumped-parameter* model. [8]

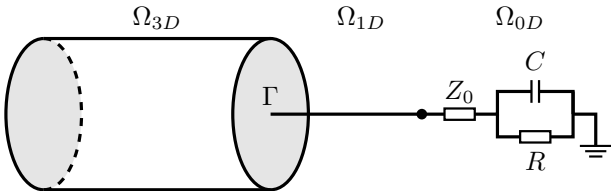


Fig. 2: Illustration of a 3D-1D model of an artery, coupled to a zero-dimensional, three-element Windkessel model. (Adapted from [9])

This would allow for simulations of the whole circulatory

system as a combination of zero-, one- and three-dimensional coupled partitions. Kim et al. [10] construct a patient-specific geometric multi-scale model of an aorta and its surrounding vascular structures by introducing a lumped-parameter model of the heart as an inflow boundary condition and using a three-element Windkessel model for the downstream circulation (Figure 2). They use this model to simulate a surgical procedure and to investigate the effects of the treatment.

One has to keep in mind, however, that local changes in the circulatory system often induce changes in the global blood flow distribution. Therefore, simulating surgical interventions or pathological alterations comes with the caveat that some parameters of the model might need to be modified. [9] In an effort to investigate this issue, Blanco et al. [11] expanded a closed-loop geometric multi-scale representation of the entire cardiovascular system by a zero-dimensional model of the baroreceptor reflex mechanism, i.e., the reflex responsible for homeostatic regulation. Thereby, they obtain a self-regulating model, which allows to explore the interplay of local and global phenomena with a high level of physiological realism.

III. NUMERICAL ASPECTS

In the literature, the spatial decomposition of geometric multi-scale models is often differentiated into two distinct types: the domain-decomposition and the domain-overlapping approach. The former is characterized by two or more separate domains only connected at the coupling interface, which is the only place where data exchange occurs. Each split domain also typically employs a different type of solver. Contrastingly, in the domain-overlapping approach the undivided system is simulated by a single method, with some specific areas of the domain additionally being computed using more refined models. The more accurate higher-dimensional data is then usually mapped onto the lower-dimensional domain of the full system. [4]

In the following section, the scope of discussion will be limited to the domain-decomposition approach, since analysis of the domain-overlapping approach is readily reduced to questions of appropriate data mapping.

A. 3D-1D Coupling

Sticking with the topic of hemodynamics, let us first consider a 1D model of a cylindrical blood vessel, obtained from integrating the Navier-Stokes equations over each section perpendicular to the z -axis, i.e., the flow direction, which yields [12]

$$\begin{aligned} \frac{\partial A}{\partial t} + \frac{\partial Q}{\partial z} &= 0, \\ \frac{\partial Q}{\partial t} + \frac{\partial}{\partial z} \left(\alpha \frac{\partial Q^2}{\partial A} \right) + \frac{A}{\rho} \frac{\partial \bar{p}}{\partial z} + K_R \frac{Q}{A} &= 0. \end{aligned} \quad (1)$$

Here, $A = A(t, z)$ describes the area of the section at location z at time t , while $Q = Q(t, z)$ and $\bar{p} = \bar{p}(t, z)$ are the associated flux and mean pressure respectively. K_R is a constant related to fluid viscosity and α corrects for the error that stems from the usage of averaged quantities

when computing the flux of momentum. To simplify, α can be considered a constant as well. To close the above system of two equations in three unknowns, i.e., A , Q and \bar{p} , a simple algebraic relation relating the area of the cylinder A to the mean pressure \bar{p} is introduced, namely

$$\bar{p} = p_{ext} + \psi(A) \text{ with } \frac{d\psi}{dA} > 0 \text{ and } \psi(A_0) = 0, \quad (2)$$

where p_{ext} denotes the constant external pressure and A_0 is the reference area. [12]

For the 3D representation of the artery we choose a compliant tube, described by the incompressible Navier-Stokes equations (3) coupled to an arbitrary structural model, which provides the radial displacement of the walls. The mathematical description of the structural model is omitted here for the sake of conciseness, but the interested reader may refer to Formaggia et al. [12]

$$\begin{aligned} \rho \frac{\partial u}{\partial t} + \rho u \nabla u - \nabla(\mu \nabla u) + \nabla p &= 0, \\ \nabla u &= 0. \end{aligned} \quad (3)$$

In equation (3), $u = u(x, y, z, t)$ denotes the velocity field, $p = p(x, y, z, t)$ is the pressure and ρ and μ stand for the density and viscosity of the fluid.

Now we consider the two domains Ω_{3D} and Ω_{1D} , belonging to the three-dimensional and the one-dimensional model respectively, connected via an interface Γ . Rationally, continuity of the following variables on Γ would be feasible: [13]

- (i) Area: $A_{3D}^\Gamma = A_{1D}^\Gamma$
- (ii) Mean pressure: $\bar{p}_{3D}^\Gamma = \bar{p}_{1D}^\Gamma$
- (iii) Flux: $Q_{3D}^\Gamma = Q_{1D}^\Gamma$
- (iv) Mean total pressure: $\bar{p}_{3D} + \frac{1}{2}\bar{u}_{3D}^2 = \bar{p}_{1D} + \frac{1}{2}\bar{u}_{1D}^2$
- (v) Incoming characteristic (*vide infra*)

However, it must be ensured that the choice of interface coupling conditions still produces two well-posed problems on either of the coupled domains, since they will be solved individually. The conditions (i) - (v) also depend on each other to some degree. Choosing conditions (i), (ii) and (v) would lead to condition (iii) being fulfilled, since (ii) and (v) imply continuity of the mean axial velocity $\bar{u} = \frac{Q}{A}$ on Γ . For the set of conditions (i), (iii) and (v) condition (ii) also follows from the continuity of \bar{u} , which is assured by (i) and (iii). [12]

Furthermore, we can reformulate some of the aforementioned conditions, due to the fact that the 1D model partially neglects viscous terms. The mean pressure of the 3D model can therefore also be interpreted as a mean normal stress $\bar{\sigma}$ and continuity of the averaged normal stress may replace condition (ii), which would also lead to a different expression for the incoming characteristic variable and the mean total pressure: [12], [13]

- (ii*) Mean normal stress: $\bar{\sigma}_{3D}^\Gamma = \bar{p}_{1D}^\Gamma$
- (iv*) Mean total pressure: $\bar{\sigma}_{3D} + \frac{1}{2}\bar{u}_{3D}^2 = \bar{p}_{1D} + \frac{1}{2}\bar{u}_{1D}^2$
- (v*) Incoming characteristic variable expressed w.r.t. $\bar{\sigma}$

From the above considerations, one can find the sets of independent interface coupling conditions listed below. While they do not necessarily provide mathematically inequivalent options, the needed numerical schemes might still differ for each choice. [13]

- (1) {(i), (ii), (v)}
- (2) {(i), (iii), (v)}
- (3) {(i), (ii*), (v*)}
- (4) {(i), (iii), (v*)}
- (5) {(i), (iv), (v)}
- (6) {(i), (iv*), (v)}

For less comprehensive models, e.g., a rigid pipe, where the area A is constant in time and space, condition (i) is fulfilled by construction of the model and condition (ii) reduces itself to the continuity of \bar{u} on Γ .

The aforementioned points, however, do not yet ensure well-posedness of the individual subsystems, especially when considering a flow from a 1D model to a three-dimensional one. Using the averaged values obtained from the one-dimensional side as a boundary condition on the interface for the 3D problem does not suffice to guarantee the uniqueness of its solution. Therefore, the mean data needs to be transformed to pointwise conditions on Γ . For this transformation a shape, e.g., a velocity profile, needs to be assumed. Considering condition (iii) for a 1D-3D fluid-fluid simulation, one could employ the Poiseuille velocity field, which – assuming Γ has a circular shape with radius R and lies in the xy -plane – is given by [13]

$$\begin{aligned} u_x &= 0, u_y = 0, \\ u_z(x, y, t) &= \frac{2Q_{1D}(t)}{\pi\rho R^2} \left(1 - \frac{(x - x_c)^2 + (y - y_c)^2}{R^2} \right), \end{aligned} \quad (4)$$

with Q_{1D} denoting the flux transferred to the interface by the one-dimensional side. Equation (4) enables the transformation of average values to pointwise Dirichlet boundary conditions on Γ for the three-dimensional problem (Figure 3), but the choice of such a velocity profile is highly arbitrary and needs to be adjusted to the geometric multi-scale problem at hand.

B. The Role of Characteristics and Spurious Effects

As previously mentioned, continuity of the characteristic variables on the interface is one of the possible choices to impose as an interface boundary condition. To explain the notion of characteristic variables, also called Riemann variables, and investigate them further let us assume a one-dimensional propagative system given by the following equations [14]

$$\frac{\partial U}{\partial t} + H(U) \frac{\partial U}{\partial z} + B(U) = 0, \quad z \in (0, \ell), \quad t > 0, \quad (5)$$

with

$$\begin{aligned} H(U) &= \begin{pmatrix} 0 & 1 \\ c_1^2 - \alpha(\frac{Q}{A})^2 & 2\alpha\frac{Q}{A} \end{pmatrix} \text{ and} \\ B(U) &= \begin{pmatrix} 0 \\ K_r \frac{Q}{A} + \frac{A}{\rho_f} \frac{\partial \psi}{\partial A_0} \frac{\partial A_0}{\partial z} + \frac{A}{\rho_f} \frac{\partial \psi}{\partial \beta} \frac{\partial \beta}{\partial z} \end{pmatrix} \end{aligned} \quad (6)$$

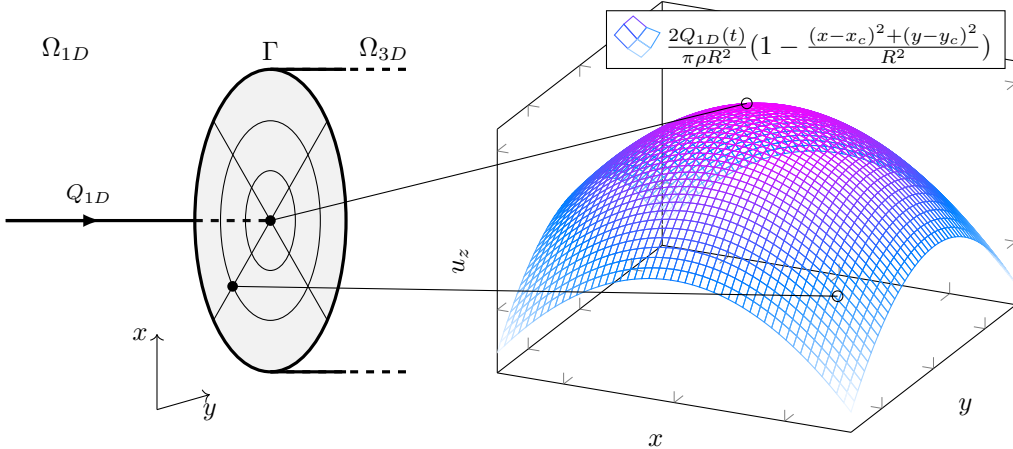


Fig. 3: Illustration of the mapping procedure to obtain pointwise Dirichlet conditions on Γ that satisfy a physical velocity profile for the three-dimensional problem from the averaged data of the 1D model, when the flow direction is going from the latter to the former.

being the flux matrix and the dissipation vector respectively. In equations (5) and (6), $U = \begin{pmatrix} A \\ Q \end{pmatrix}$ is the vector of the unknowns area A and flux Q , ℓ is the length of the system, t denotes time, α is the Coriolis coefficient, also known as momentum flux correction coefficient, K_r is the friction parameter, ψ is the relation of pressure and area (compare equation (2)), and $c_1 = \sqrt{\frac{A}{\rho_f} \frac{\partial \psi}{\partial A}}$.

We can now introduce $L = \begin{pmatrix} l_1^T \\ l_2^T \end{pmatrix}$ and $R = (r_1 \ r_2)$, with l_1, l_2, r_1, r_2 as the left and right eigenvectors of H respectively. This leads us to the definition of the characteristic variables, denoted as W_1 and W_2 , given by [14]

$$\begin{aligned} \frac{\partial W_1}{\partial U} &= l_1, \\ \frac{\partial W_2}{\partial U} &= l_2. \end{aligned} \quad (7)$$

It is important to note that an explicit expression of W_1 and W_2 depending on the physical variables of the system can generally be found. For the above system, one finds

$$W_{1,2} = \frac{Q}{A} \pm 4 \sqrt{\frac{\beta}{2\rho_f A_0}} A^{\frac{1}{4}}, \quad (8)$$

where β depends on the Young modulus, the Poisson modulus and the thickness of the wall membrane. [14] However, these expressions are determined by the chosen model and its parameters. Without delving any deeper into the underlying mathematics, it shall be summarized that characteristics define the propagation properties of the system and play an important role in determining the flow behavior. Since the incoming and outgoing characteristics carry information about the flow, it is desirable to impose continuity of these variables on the interface by setting the outgoing characteristic of the upstream domain equal to the incoming characteristic of the downstream domain. By employing characteristic variables, one can increase the physicality of the simulation and reduce

spurious effects, such as unphysical reflections at the outflow boundary. [15]

IV. SIMULATION: 1D-3D PARTITIONED PIPE

A 1D-3D geometric multi-scale model of non-compressible flow in a rigid pipe was implemented and simulated. [16] The following section addresses the underlying models and discusses the obtained results.

A. 1D Model

The incompressible flow in the one-dimensional domain Ω_{1D} is described by the Euler equations, given by

$$\begin{aligned} \frac{\partial u}{\partial x} &= 0, \\ \frac{\partial u}{\partial t} + \frac{\partial p}{\partial x} &= 0, \end{aligned} \quad (9)$$

where u denotes the velocity, p is the pressure and x and t are the spatial and temporal coordinates respectively.

To solve this system, one first discretizes the second equation in time using an explicit Euler step with time step size τ , yielding

$$u^{n+1} = u^n - \tau \frac{\partial p}{\partial x}. \quad (10)$$

The only unknown left, that is needed to compute the new velocity u^{n+1} is the related pressure $p = p^{n+1}$. Inserting into the continuity equation, i.e., the first part of the Euler equations, leads to

$$\frac{\partial u^{n+1}}{\partial x} = \frac{\partial u^n}{\partial x} - \tau \frac{\partial^2 p^{n+1}}{\partial x^2} = 0. \quad (11)$$

The above equation can be rearranged to

$$\frac{\partial^2 p^{n+1}}{\partial x^2} = \frac{1}{\tau} \frac{\partial u^n}{\partial x}, \quad (12)$$

which is the one-dimensional Pressure Poisson Equation (PPE), and can be solved using, e.g., a successive-over-relaxation solver.

With the obtained pressure values one can solve for the updated velocities u^{n+1} by using a forward difference approach to approximate the spatial derivative. This leaves us with

$$u_i^{n+1} = u_i^n - \tau \left(\frac{p_{i+1}^n - p_i^n}{h} \right), \quad (13)$$

where h denotes the mesh size.

The boundary conditions on the inlet are chosen to be a Dirichlet boundary condition for the velocity and a Neumann boundary condition for the pressure. On the outlet they are chosen vice versa.

B. 3D Model

The 3D cylindrical pipe model is implemented in OpenFOAM [17], [18], using the pimpleFoam finite volume solver for incompressible flows. It consists of an inlet with a fixed-value velocity boundary condition and a fixed-gradient pressure boundary condition. On the walls of the cylinder, a no-slip condition is enforced. The outlet has a fixed-value pressure, and a fixed-gradient velocity boundary condition. The simulation employs a Newtonian transport model, that considers the viscosity to be constant.

C. Coupling and Interface

The coupling of the 1D and the 3D model was achieved by using preCICE [19], [20], in particular its OpenFOAM adapter [21] and Python language-bindings. The two solvers are coupled serial-implicitly, which means that each solver iterates each time step until both are converged, up to a specified tolerance. A Quasi-Newton acceleration technique, namely Anderson acceleration, was used for the 3D solver. The solvers share velocity and pressure values with each other, with the 1D model writing its outlet-velocity to the inlet of the 3D solver, while reading the inlet-pressure, written by the 3D simulation, to its outlet (Figure 4). The combined model is akin to the scheme used to illustrate the general idea of geometric multi-scale models (Figure 1).

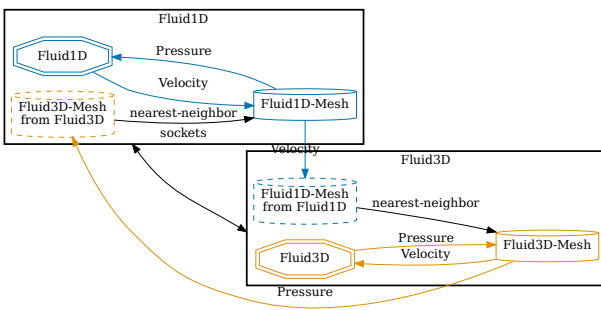


Fig. 4: Visualization of the configuration used to couple the dimensionally heterogeneous flow models via preCICE. The velocity and pressure data is first written to the respective interface meshes (depicted in the figure as cylinders), from which they are mapped to each other via nearest-neighbor mapping. Afterwards, the required data, i.e., velocity for Fluid3D and pressure for Fluid1D, is read from the respective interface mesh. [22]

The data mapping between the interface meshes is based on a consistent nearest-neighbor mapping procedure. Consistency in this context describes that the singular values from one mesh are exactly transcribed to the other mesh, while, for example, conservative mapping would preserve the cumulative value of all mapped data. Since the 3D domain requires vector-valued velocities u , the 1D solver shares its velocity data as a vector consisting of only the z -component, i.e., the principal flow direction. The simulation does therefore not enforce a velocity profile at the inlet of the 3D domain, as previously considered in the section on 3D-1D coupling. The implications of this will be addressed when discussing the results.

D. Results and Discussion

The simulation was run from a starting time of $t = 0$ up to an end time of $t = 1$, with a time step size of $\delta t = 0.01$. The results for selected time frames are shown in Figure 5 and Figure 6.

As can be seen in Figure 5, the flow formation happens rather quickly and homogeneously along the length of the pipe. Figure 5 (d) even shows that the inlet velocity is already matched inside the domain at a time of $t = 0.30$. However, comparison to Figure 6, especially Figure 6 (e), suggests that the maximum velocity of the pipe flow is not reached. This is because the solutions of the 1D solver have to be considered average velocities of the laminar tube flow.

Figure 6 depicts the build-up of a laminar velocity profile that can be observed fully formed in Figure 6 (d), at a time of $t = 0.30$. Even after its formation, however, there remains a layer of fluid with uniform velocity near the inlet. This can be attributed to the omission of transforming the averaged velocities obtained from the 1D solver to boundary conditions that fulfill a laminar velocity profile. By implementing such a transformation, the boundary layer at the inlet of the 3D domain can be eliminated, as can be seen in Figure 7. Employing this transformation of boundary velocities also leads to a fully linear pressure drop in the three-dimensional domain, instead of having non-linear artifacts near the inflow boundary (Figure 8).

Figures 9 and 10 show the pressure and velocity data obtained from the geometric multi-scale pipe flow model in comparison to the results of a purely three-dimensional monolithic counterpart, that were obtained from an OpenFOAM simulation. To be exact, the plots only show values extracted along the z -axis, i.e., the principal flow direction.

The monolithic simulation seemingly displays a quicker formation of flow than the geometric multi-scale model, since at a time of $t = 0.01$, higher velocity values than the inlet velocity can already be observed in latter parts of the reference pipe model. The velocity values of the dimensionally heterogeneous model, however, stay fairly close to zero. It can also be seen that the velocity boundary condition shows at the inlet for the 1D domain, which seems to lead to a step discontinuity (Figure 9 (a)). At a time of $t = 0.50$, when the laminar velocity profile is fully formed, it is clearly visible that the one-dimensional solver yields the average laminar flow

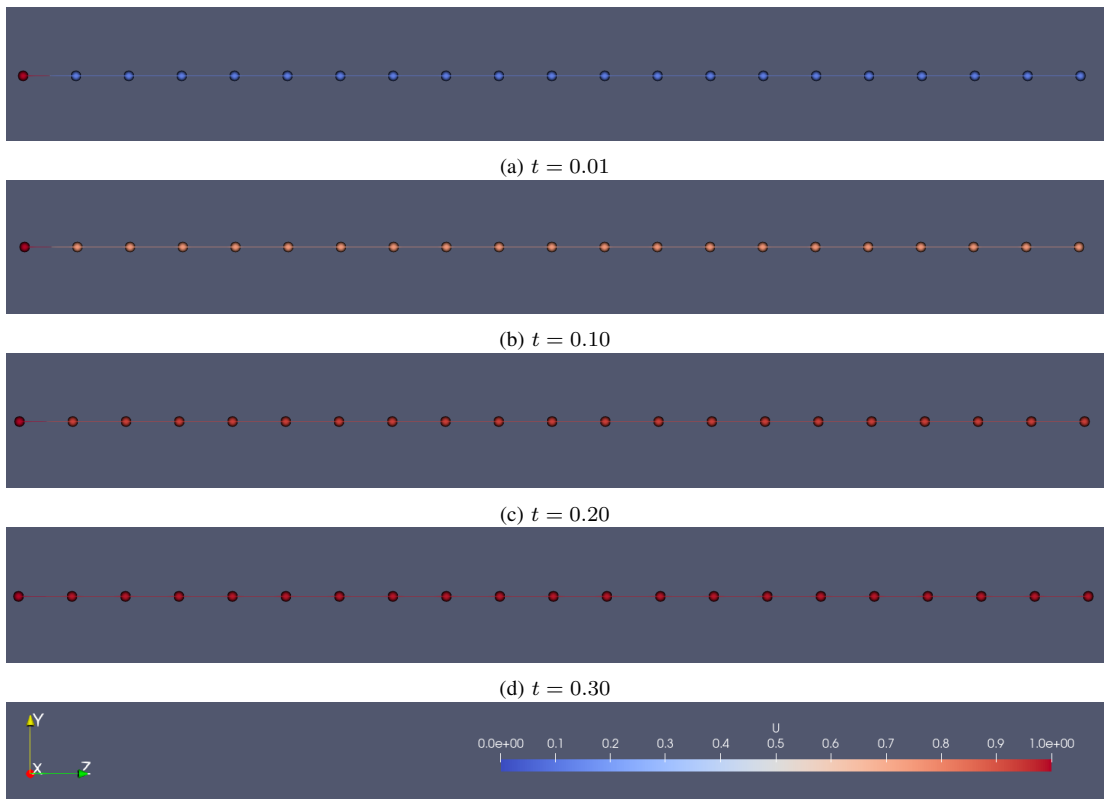


Fig. 5: Calculated velocity values of the 1D solver along 21 nodes at selected time frames.

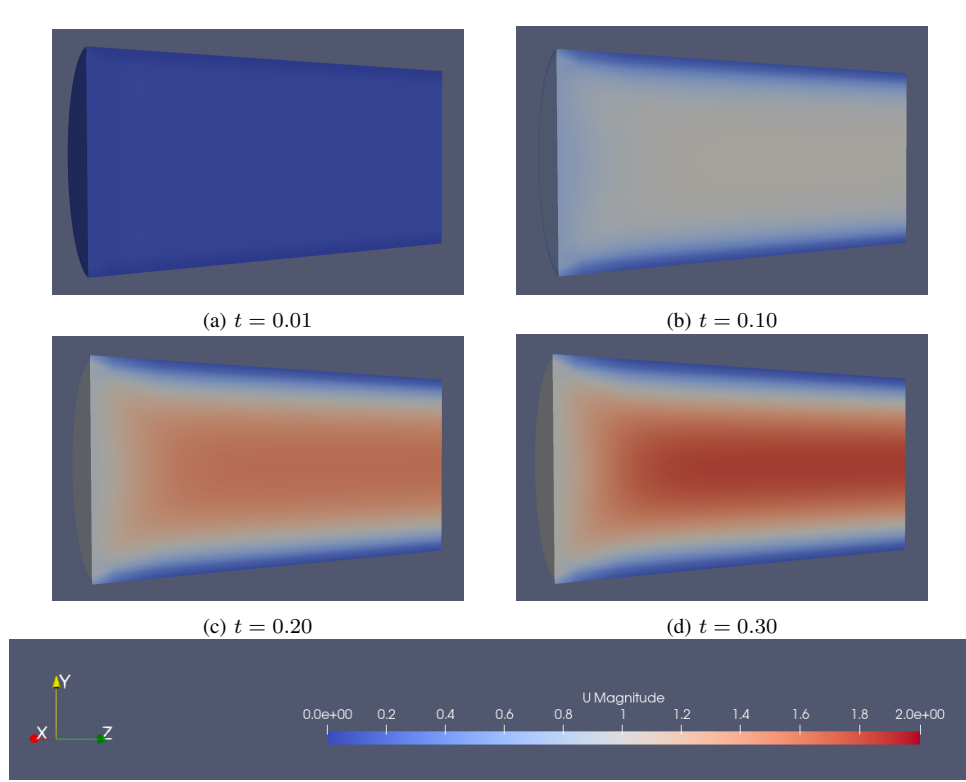


Fig. 6: Velocity values obtained from the 3D solver at selected time frames.

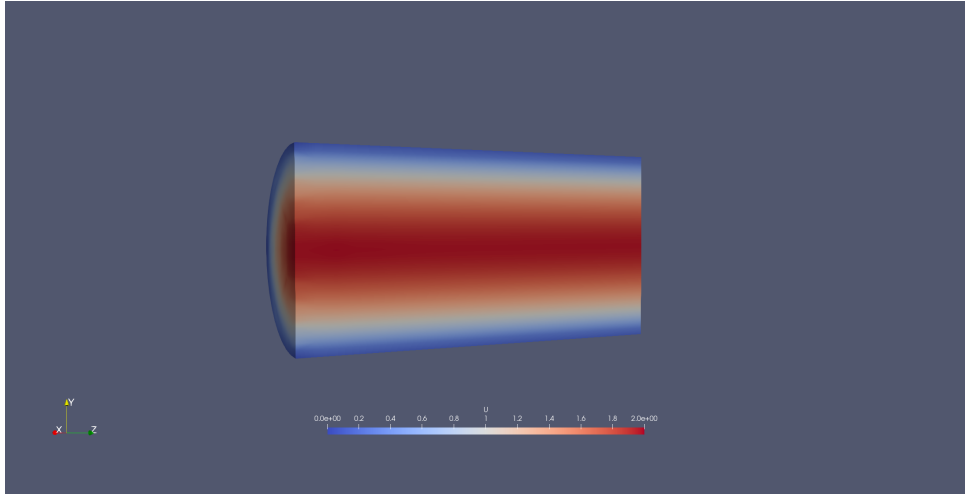


Fig. 7: Visualization of the result of the 3D simulation at time $t = 0.50$ with an implemented transformation of 1D velocity values to point-wise Dirichlet conditions that fulfill a laminar velocity profile for the inlet of the three-dimensional pipe.

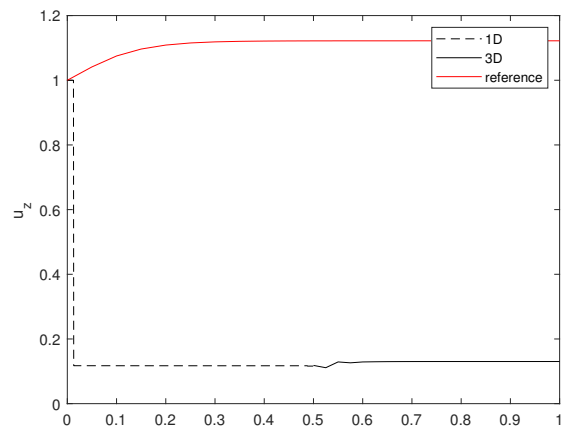
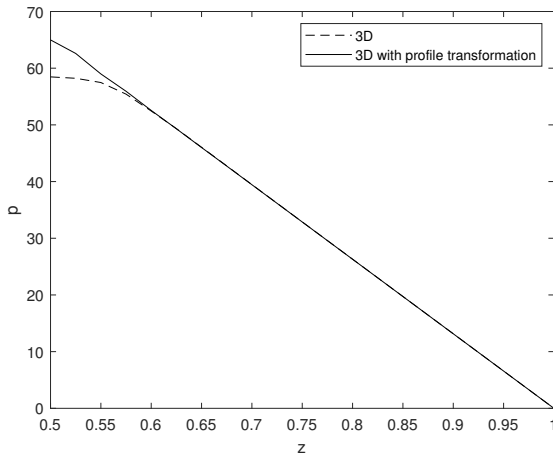
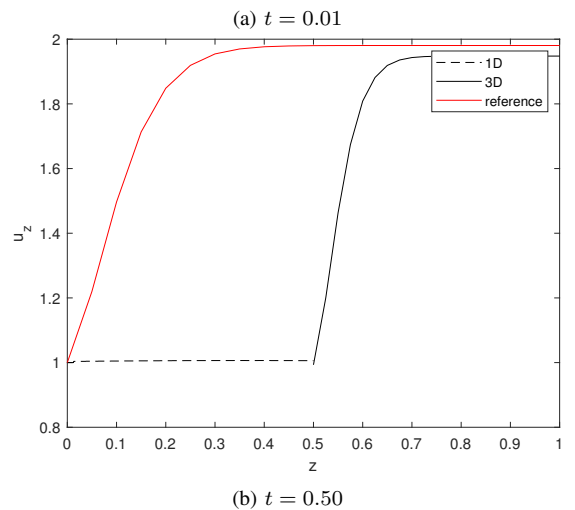


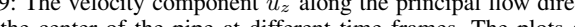
Fig. 8: The pressure value p along the principal flow direction z at the center of the three-dimensional pipe with and without transformation of 1D velocity values to point-wise Dirichlet conditions that fulfill a laminar velocity profile at the interface boundary. The position $z = 0.5$ is the interface position.

velocity, which is exactly half of the maximum velocity of $u_z = 2$ that can be observed for the reference, but also the 3D solver. The aforementioned boundary layer of lower velocity near the inlet of the 3D domain can also be seen in Figure 9 (b), which indicates an unphysical build-up of a velocity profile.

As for the pressure data, Figure 10 reveals significant shortcomings of the one-dimensional flow solver. While at a time of $t = 0.01$, the pressure at the outlet of the 1D domain still matches with the inlet pressure of the 3D domain, as imposed by the boundary condition. Later, at $t = 0.50$, the pressure of the one-dimensional pipe equals zero everywhere. The geometric multi-scale model tends to overestimate the pressure compared to the pressure of the reference simulation. It is also unexpected to see homogeneous pressure along the 1D domain at the earlier time frame. This might stem from the



(a) $t = 0.01$



(b) $t = 0.50$

Fig. 9: The velocity component u_z along the principal flow direction z at the center of the pipe at different time frames. The plots show the data obtained from the geometric multi-scale model compared to a monolithic 3D pipe flow simulation conducted in OpenFOAM, labelled in the plots as reference and shown in red. For the sake of clarity, the data was scaled such that the pipe has a length equal to $z = 1$, with the interface position being $z = 0.5$.

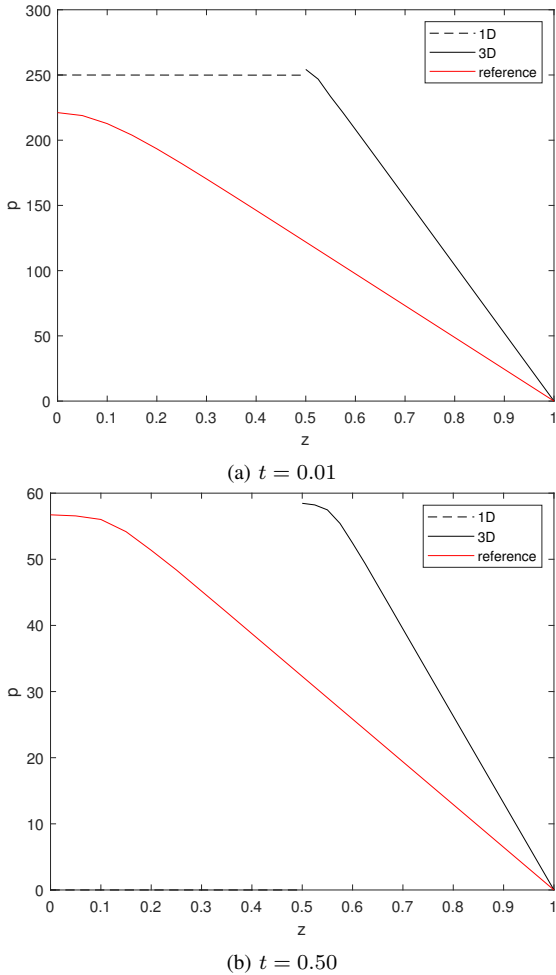


Fig. 10: The pressure value p along the principal flow direction z at the center of the pipe at times of $t = 0.01$ and $t = 0.50$. The plots show the data obtained from the geometric multi-scale model compared to a monolithic 3D pipe flow simulation conducted in OpenFOAM, labelled in the plots as reference and shown in red. For the sake of clarity, the data was scaled such that the pipe has a length equal to $z = 1$, with the interface position being $z = 0.5$.

problem of solving for the pressure not being well posed with changing boundary conditions, which could be alleviated by simply imposing a zero Dirichlet condition instead of reading the pressure from the 3D solver. It might also merely be a bug in the solver and will need to be examined in more detail. The pressure drop along the 3D domain, however, mirrors the pressure drop of the reference results in shape and order of magnitude. Therefore, while the pressure values of the 1D solver seem to be unphysical, the 3D domain still yields results of high fidelity.

V. CONCLUSION

Geometric multi-scale models can serve as an ingenious way of reducing computational complexity and upholding flexibility in large simulations. However, the lower-dimensional models can act as a bottleneck on the fidelity of the overall simulation results, as can be seen for the 1D-3D partitioned

pipe simulation, where the 1D solver produced erroneous pressure data. Keeping in mind that one ought to be careful which parts of a desired domain can be substituted for reduced models is therefore essential and can make or break the quality of the obtained data. This consideration, of course, requires in-depth knowledge of the processes at hand and a certain level of expertise. Are these requirements met, there's plenty of opportunities of employing geometric multi-scale coupling, especially for the flow problems discussed extensively in previous sections. Nevertheless, not being aware of potential pitfalls can seriously harm the physicality of the simulation results, as shown by the data obtained with a velocity profile agnostic interface. Since the coupling procedure is fairly simple, with the exception of some caveats regarding the type of data different simulations yield (e.g., transforming the 1D velocity data to 3D vectors and imposing a velocity profile), it can also be done by simulation researchers without extensive software engineering proficiency and could enable them to either reduce the computational cost of their models or refine certain areas of interest with higher-fidelity solvers. This could be of potential interest not only in nuclear engineering and hemodynamics, but also research areas such as climate modeling, chemical engineering, material science or computational physics.

REFERENCES

- [1] W. de Paula Ferreira, F. Armellini, and L. A. de Santa-Eulalia, “Simulation in industry 4.0: A state-of-the-art review,” *Computers & Industrial Engineering*, vol. 149, no. 3, p. 106868, 2020.
- [2] G. Lerchl, H. Austregesilo, P. Schöffel, D. Von der Cron, and F. Weyermann, “ATHLET mod 3.0—Cycle A. user’s manual,” *Gesellschaft für Anlagen-und Reaktorsicherheit (GRS), Garching bei München, Germany, Report No. GRS-P-1*, vol. 1, 2012.
- [3] D. Tenchine, R. Baviere, P. Bazin, F. Ducros, G. Geffraye, D. Kadri, F. Perdu, D. Piella, B. Rameau, and N. Tauveron, “Status of CATHARE code for sodium cooled fast reactors,” *Nuclear Engineering and Design*, vol. 245, pp. 140–152, 2012. [Online]. Available: <https://www.sciencedirect.com/science/article/pii/S0029549312000520>
- [4] T. P. Grunloh and A. Manera, “A novel domain overlapping strategy for the multiscale coupling of CFD with 1D system codes with applications to transient flows,” *Annals of Nuclear Energy*, vol. 90, pp. 422–432, 2016.
- [5] M. Zanetti, A. Cammi, C. Fiorina, and L. Luzzi, “A geometric multiscale modelling approach to the analysis of MSR plant dynamics,” *Progress in Nuclear Energy*, vol. 83, no. 0, pp. 82–98, 2015.
- [6] J. Serp, M. Allibert, O. Beneš, S. Delpech, O. Feynberg, V. Ghetta, D. Heuer, D. Holcomb, V. Ignatiev, J. L. Kloosterman, L. Luzzi, E. Merle-Lucotte, J. Uhlíř, R. Yoshioka, and D. Zhimin, “The molten salt reactor (MSR) in generation IV: Overview and perspectives,” *Progress in Nuclear Energy*, vol. 77, no. 1–3, pp. 308–319, 2014.
- [7] S. Mendis, P. Puska, B. Norrvig, W. H. Organization, W. H. Federation, and W. S. Organization, “Global atlas on cardiovascular disease prevention and control / edited by: Shanthi mendis ... [et al.],” p. Published by the World Health Organization in collaboration with the World Heart Federation and the World Stroke Organization, 2011.
- [8] T. Passerini, M. d. Luca, L. Formaggia, A. Quarteroni, and A. Veneziani, “A 3D/1D geometrical multiscale model of cerebral vasculature,” *Journal of Engineering Mathematics*, vol. 64, no. 4, pp. 319–330, 2009.
- [9] L. Taelman, J. Degroote, P. Verdonck, J. Vierendeels, and P. Segers, “Modeling hemodynamics in vascular networks using a geometrical multiscale approach: numerical aspects,” *Annals of Biomedical Engineering*, vol. 41, no. 7, pp. 1445–1458, 2013.
- [10] H. J. Kim, I. E. Vignon-Clementel, C. A. Figueroa, J. F. LaDisa, K. E. Jansen, J. A. Feinstein, and C. A. Taylor, “On coupling a lumped parameter heart model and a three-dimensional finite element aorta model,” *Annals of Biomedical Engineering*, vol. 37, no. 11, pp. 2153–2169, 2009.

- [11] P. Blanco, P. Trenhago, L. Fernandes, and R. Feij  o, “On the integration of the baroreflex control mechanism in a heterogeneous model of the cardiovascular system,” *International Journal for Numerical Methods in Biomedical Engineering*, vol. 28, no. 4, pp. 412–433, 2012.
- [12] L. Formaggia, J. Gerbeau, F. Nobile, and A. Quarteroni, “On the coupling of 3D and 1D Navier–Stokes equations for flow problems in compliant vessels,” *Computer Methods in Applied Mechanics and Engineering*, vol. 191, no. 6, pp. 561–582, 2001.
- [13] L. Formaggia, A. Quarteroni, and A. Veneziani, *Cardiovascular mathematics: Modeling and simulation of the circulatory system / Luca Formaggia, Alfio Quarteroni, Alessandro Veneziani, (eds.)*, ser. MS&A. Milan: Springer, 2009, vol. v. 1.
- [14] A. Quarteroni, A. Veneziani, and C. Vergara, “Geometric multiscale modeling of the cardiovascular system, between theory and practice,” *Computer Methods in Applied Mechanics and Engineering*, vol. 302, no. 1, pp. 193–252, 2016.
- [15] C. Hirsch, *Numerical computation of Internal and External Flows, Volume 2: Computational Methods for Inviscid and Viscous Flows*. Chichester: Wiley, 1988-90.
- [16] Code available at <https://gitlab.lrz.de/000000000149ACB8/>
1d-3d-partitioned-pipe-simulation.
- [17] H. G. Weller, G. Tabor, H. Jasak, and C. Fureby, “A tensorial approach to computational continuum mechanics using object-oriented techniques,” *Computer Methods in Applied Mechanics and Engineering*, vol. 12, no. 6, p. 620, 1998.
- [18] <https://openfoam.org>, last accessed: 12.01.2022.
- [19] H.-J. Bungartz, F. Lindner, B. Gatzhammer, M. Mehl, K. Scheufele, A. Shukaev, and B. Uekermann, “preCICE – a fully parallel library for multi-physics surface coupling,” *Computers and Fluids*, vol. 141, pp. 250–258, 2016, advances in Fluid-Structure Interaction.
- [20] <https://precice.org>, last accessed: 12.01.2022.
- [21] Gerasimos Chourdakis. A general OpenFOAM adapter for the coupling library preCICE. *Master's thesis*, Department of Informatics, Technical University of Munich, 2017.
- [22] <https://github.com/precice/config-visualizer>, last accessed: 21.01.2022.